Journal of Applied Electrochemistry (2022) 52:247–258
https://doi.org/10.1007/s10800-021-01641-2

RESEARCH ARTICLE

An easy synthesis of carbon-supported silver–cobalt bimetallic nanoparticles to study the electrocatalytic performance in alkaline borohydride fuel cell

Santanu Dey[1] · Subhamay Pramanik[2] · Pradipta Chakraborty[1,3] · Dhiraj Kumar Rana[1] · Soumen Basu[1]

Received: 24 May 2021 / Accepted: 24 October 2021 / Published online: 2 November 2021

Abstract

Here, we report a cost-effective non-platinum carbon-supported electrocatalyst based on silver–cobalt (Ag–Co) bimetal which is infrequently reported as electrocatalyst in fuel cell application. Carbon-supported Ag–Co bimetallic nanoparticles were synthesized with three different metal loadings in aqueous medium using reduction method to use in direct borohydride fuel cell as the anode catalyst. The crystalline structure, composition, and morphology of the synthesized samples (S-1, S-2, and S-3) were characterized by X-ray diffraction spectroscopy, X-ray photoelectron spectroscopy, and field emission scanning electron microscopy. The electrocatalytic characterizations of Ag–Co/C in 0.5 M NaOH and 0.5 M NaOH + 0.01 M $NaBH_4$ were carried out by cyclic voltammetry, electrochemical impedance spectroscopy, and chronoamperometry measurements. The principle electrochemical kinetics parameters (e.g., current density, number of exchange electrons, and apparent activation energy) toward borohydride oxidation on Ag–Co/C electrocatalyst were evaluated. Results confirm that the borohydride electro-oxidation performance is greater for S-1 electrocatalyst in terms of oxidation current density and onset potential. The number of exchange electrons for S-1, S-2, and S-3 catalysts in 0.5 M NaOH + 0.01 M $NaBH_4$ solution at 25 °C was calculated as 1.95, 1.10, and 0.17, respectively. The apparent activation energy at S-1-modified electrode surface was evaluated as 31.86 kJ mol^{-1}.

Graphic abstract

CV of Ag–Co bimetallic electrocatalyst in 0.5 M NaOH solution at different scan rates at 25 °C nanoparticles.

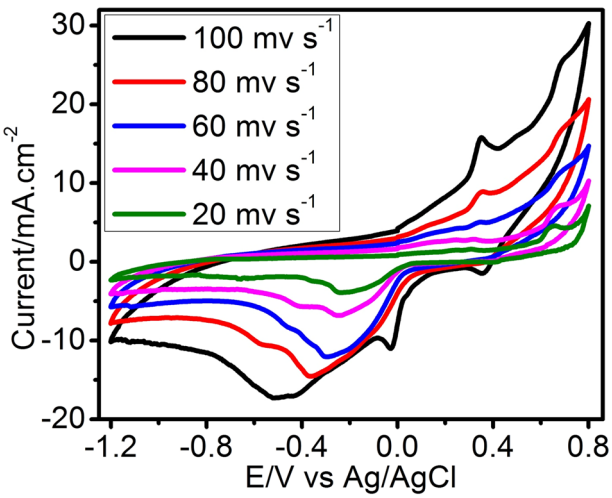

Keywords Direct borohydride fuel cell (DBFC) · Ag–Co/C nanoparticles · Borohydride oxidation · Stability · Apparent activation energy · Number of exchange electrons

Extended author information available on the last page of the article

1 Introduction

Due to global growing environmental pollution and diminution of fossil fuel sources, the search of new power sources get high attention in recent past. Fuel cells have drawn huge interest because of their capability to impart a risk free and efficient way of energy production. Feeding with alcohols (like methanol, ethanol, ethylene glycol) or borohydride in direct liquid fuel cells has been studied as an alternative of hydrogen fuel cell [1–3]. Although direct methanol fuel cell (DMFC) and direct borohydride fuel cell (DBFC) both can remove the hydrogen storage problem, DBFC beats DMFC in terms of theoretical open-circuit voltage, electrochemical activity, capacity value, and power performance at ambient temperature [4]. Moreover, DBFC employs alkaline solution as fuel that has comparatively less corrosion activity and then it is feasible to use commercially using cost effective and easily available metal nanoparticles as anode catalysts.

Nowadays, use of sodium borohydride ($NaBH_4$) in direct liquid fuel cells as anode fuel has attracted large attention due to its good hydrogen content (10.6 wt%), non-toxicity, and enough chemical stability in alkaline medium and it is easy to handle [5]. Additionally, complete oxidation of $NaBH_4$ produces eight electrons (following Eq. 1) that is higher than the number of electrons generated in the electro-oxidation of hydrazine [6], methanol [7], ethanol [8], and even hydrogen [9].

$$BH_4^- + 8OH^- \rightarrow BO_2^- + 4H_2O + 8e^- \quad (1)$$

The material of electrode is undoubtedly a key parameter in borohydride electro-oxidation where a well-capable electrocatalyst is essential. In the last few years, different metals such as Pd [10], Pt [11], Au [12], and Ag [13] have been investigated as electrocatalysts for borohydride electro-oxidation. Although, Ag is relatively cheap (60 times less cost than Pt), more abundant than other noble metals (Pd, Pt, Au, etc.), and it displays admirable electrocatalytic activity toward borohydride electro-oxidation, but Ag is not good to use alone as anode electrocatalyst for DBFC due to its low power densities and sluggish electrode kinetics [14]. Therefore, it is important to develop new efficient Ag-based catalysts with better performance.

The bimetallic electrocatalysts have been designed by combining noble metals (Pt, Pd, Au, Ag, etc.) with other non-noble metals which provide a remarkable increase in catalytic activity compared to single-component materials because of the synergistic effect of bimetal. Among the non-noble metals, nickel, cobalt, and copper have obtained much attention as electrocatalyst for borohydride electro-oxidation. Wang et al. [15] reported enhanced catalytic activity toward borohydride oxidation at PtNi/C and explain on basis of alloying effect and the change of electronic structure of Pt in presence of Ni. Feng et al. [16] synthesized Ag–Ni alloy and reported that the Ag–Ni catalyst exhibits higher capacity and discharge voltage compared to Ag in borohydride electro-oxidation. Sljukic et al. [17] compared the catalytic activity of $Pt_{0.75}M_{0.25}$ (M=Co, Ni) and Pt/C toward borohydride electro-oxidation and the investigation exposed the positive effect of presence of Co and Ni metals on the performance of Pt alloy as lower activation energies, higher number of exchange electrons, and current densities. Cobalt is recognized as a potential catalyst among transition metals for borohydride electro-oxidation, attributing to its good capacity to break B–H bonds in BH_4^- [18].

In our work, carbon-supported Ag–Co bimetallic nanoparticles were synthesized with three different metal loadings in aqueous medium using a simple chemical reduction method and used these nanoparticles as anode catalysts in DBFC. Highly porous carbon material (XC-72R carbon black) were used because of its large surface area and excellent porosity, which make the electrolyte ions easily pervade into the entire matrix surface and raise the employment of electrocatalyst surfaces [19]. The electrocatalytic performances of the synthesized bimetallic nanoparticles were studied by cyclic voltammetry (CV), electrochemical impedance spectroscopy (EIS), and chronoamperometry (CA) with different temperatures to explore the electrocatalytic activity toward borohydride oxidation.

2 Experimental

2.1 Chemicals and reagents

Double-distilled water was used to prepare all the solutions. Silver nitrate ($AgNO_3$) and cobalt nitrate [$Co(NO_3)_2{\cdot}6H_2O$] were used as metal precursors. Sodium borohydride ($NaBH_4$) was used as a reducing agent. These chemicals were purchased from Merck, India. Vulcan XC-72R was purchased from Fuel Cell Store (USA) to use as carbon source. All these materials were analytical grade reagents and used without further purification.

2.2 Synthesis of bimetallic Ag–Co/C catalysts

XC-72R powder was dispersed in 30 ml distilled water for 1 h. After that 5 ml aqueous solution of 0.084 g $AgNO_3$ and 5 ml aqueous solution of 0.145 g $Co(NO_3)_2$ were added into the carbon suspension under continuous magnetic stirring. After 30 min 5 ml aqueous solution of 0.018 g $NaBH_4$ was mixed dropwise into the previous mixture (mixture of metal precursors and carbon powder) and continued magnetic stirring for next 5 h for complete reduction of metal precursors. After that the mixture was filtered and washed several times to remove the impurities using ethanol and distilled

Table 1 Information about metal loading of synthesized electrocatalysts

Samples	Metal:carbon (weight ratio)	Ag:Co (weight ratio)
S-1	10:90	65:35
S-2	30:70	
S-3	50:50	

water. Then it is dried in oven at 70 °C for 12 h. The weight ratio of Ag to Co was fixed as 1.85 (Ag:Co = 65:35) but the amount of carbon powder was different for three different metal loadings. These samples were indexed as S-1, S-2, and S-3. The details about metal-to-carbon weight ratio of our prepared electrocatalysts are summarized in Table 1.

2.3 Physical characterizations of catalysts

The X-ray diffraction (XRD) patterns of S-1, S-2, and S-3 were observed by an X-ray diffractometer (Proto AXRD) using Cu K_α radiation (1.54 Å) for 20°–80° range of 2θ with 0.02° step size. To get XRD pattern all samples were coated on different glass slides by drop-casting to make films, and glass slides were cleaned by water, methanol, and acetone and then sonicated in double-distilled water for 10 min in an ultrasonic bath before drop-casting.

The FESEM of these as-prepared samples was explored by ZEISS Gemini SEM microscopy to investigate the morphology. The XPS was performed to investigate the compositions and element valances using PHI 5000 Versa Probe II, FEI Inc–ray electron spectrometer.

2.4 Electrocatalytic measurements of catalysts

The electrocatalytic measurements (CV, EIS, and CA) of as-prepared Ag–Co/C samples were done by a potentiostat/galvanostat (PGSTAT302N, Autolab, Metrohm). A mesh of platinum wire (1 cm × 1 cm, 50 meshes) and a 3 mol potassium chloride (KCl)-saturated Ag/AgCl electrodes were used as the counter and the reference electrode, respectively. A glassy carbon electrode (GCE) having 4 mm diameter was employed as a working electrode in this study. The GCE was cleaned properly by distilled water and ethanol all the time before each experiment. We used Nafion (Nafion™ NR 50, Merck) as a binder to prepare the catalyst ink. 55 mg of Nafion has dissolved completely in 45 ml ethanol and then 8 mg of Ag–Co/C nanopowder was mixed in the 1 ml of Nafion solution. The mixture was sonicated for 30 min in an ultrasonic bath to make a homogeneous catalyst ink. To modify the GCE surface, we dropcasted 6 µl catalyst ink and dried it for 2 h by 100 W electric bulb. The current densities were calculated according to the geometric area (0.1256 cm^2) of the working electrode. The electrolyte solutions (0.5 M NaOH and 0.5 M NaOH + 0.01 M $NaBH_4$) were prepared using double-distilled water and a one compartment borosil beaker was employed as electrolyte cell. Highly pure N_2 gas was bubbled in the electrolyte solutions for 30 min before electrocatalytic measurements to remove O_2 and CO_2 from the solutions.

3 Results and discussion

3.1 Physical characterization of Ag–Co/C catalysts

To know the crystallinity, composition, and morphology, the synthesized samples were characterized by XRD, XPS, and FESEM. Figure 1 represents the XRD pattern of the prepared samples. The obtained XRD peaks can be indexed to the (111), (200), (220), and (311) planes. Another smaller intense peak for S-1 sample at 2θ value of 25.38 was observed, which is the peak for carbon used in synthesis process. The XRD pattern of the Ag–Co/C nanoparticles is similar to the fcc structure of silver. Although, no peaks are observed due to the existence of metallic Co and Co oxides. But their existence cannot be averted. Probably they are present in amorphous form or in a very little amount [20]. The presence of cobalt was confirmed by XPS analysis.

The average crystal size of the as-prepared catalysts was calculated using Scherrer equation [21]:

$$D = \frac{0.9\lambda}{\beta cos\theta} \tag{2}$$

where D, λ, β, and θ are the mean crystal size (nm), wavelength of X-ray (1.54 Å for Cu K_α radiation), full width at half maximum (FWHM) in radians, and Bragg angle,

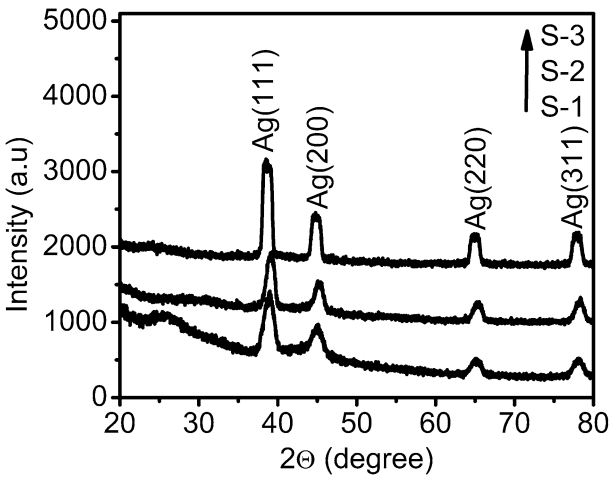

Fig. 1 XRD pattern of S-1, S-2, and S-3 electrocatalysts

respectively. The evaluated value of D for S-1, S-2, and S-3 catalysts were 5.91 nm, 9.46 nm, and 9.57 nm. The result indicates that the average crystal size can increase with the increase of metal loading in carbon-supported silver–cobalt bimetallic nanoparticles. The information extracted from XRD data is summarized in Table 2.

Figure 2 shows typical FESEM images for the prepared catalysts. The metal particles on all electrocatalysts display an agglomeration of different sizes and a roughly sphere-like shape. All particles are dispersed well on the porous carbon powder.

The XPS profile of S-1 catalyst is presented in Fig. 3. In case of core level spectrum of Ag, peaks at 368.65 eV and 374.75 eV are allocated to $Ag3d_{5/2}$ and $Ag3d_{3/2}$ transitions, respectively. The 6.10 eV spin–orbit coupling and these energies are the features of metallic silver (Ag°) [22]. A little involvement of silver oxide (Ag_2O) was noticed. But peaks corresponding to Ag_2O are absent in XRD pattern of Fig. 1, indicating that oxides are mainly in amorphous state in S-1 catalyst. In XPS spectrum relating to Co, peaks at 783.40 eV and 797.13 eV are assigned to $Co2p_{1/2}$ and $Co2p_{3/2}$ transitions, respectively, which correspond to Co^{+2} and Co^{+3}. The shoulders at 785.69 eV and 801.25 eV are satellite signals related to Co^{+2} only. This is consistent with the previous literature data [20].

3.2 Electrocatalytic performances of Ag–Co/C

At first, CV was performed of our synthesized samples in 0.5 M NaOH solution. Figure 4 exhibits the CV profile versus Ag/AgCl in 0.5 M NaOH solution at 100 mV s^{-1} scan rate at 25 °C. It seems that there was no proper oxidation–reduction peaks on the unmodified glassy carbon electrode, indicating that glassy carbon was stable in alkaline solution. But the redox peaks were readily observed on S-1, S-2, and S-3-tailored glassy carbon electrode surfaces. The curves display clear anodic peaks at 0.45 V, 0.35 V, and 0.31 V for S-1, S-2, and S-3 electrodes, respectively. There were other very small anodic humps on S-2- and S-3-modified electrode surfaces at around 0.7 V. These anodic features are credited to electrochemical adsorption of OH^- and formation of silver oxide layers on electrode surfaces [20, 23]. The S-1-modified electrode showed two cathodic peaks centered at 0.32 V and − 0.2 V. Similar cathodic features were observed at 0.36 V and 0.02 V on S-3 electrode surface. The S-2-modified electrode showed three cathodic peaks centered at 0.35 V, − 0.02 V, and a very broad hump at 0.51 V. These cathodic peaks accredited to the reduction of hydroxides and oxides produced under anodic circumstances into elemental Co and Ag [23, 24]. Inset of Fig. 4 shows the CV of 20 wt% Ag/C-modified glassy carbon electrode in identical condition. Results confirmed that the Ag–Co/C-modified electrode has higher electrocatalytic activity than 20 wt% Ag/C. This is because the presence of Co is involved in increasing electron conduction in the carbon-supported bimetallic system [25]. Besides, comparison of the CVs on Ag/C and Ag–Co/C electrode shows further negative sweep of potentials in the reduction peak measured during the backward scan for the bifunctional material, suggesting a stronger O_{ad} interaction with Ag surface sites in the presence of Co which could assist the breaking of the oxygen–oxygen (O–O) bond [26]. Results also show that S-1-modified electrode has better electrochemical anodic activity than other synthesized materials.

To realize the effect of scan rate on electrocatalytic performance, we carried out CV at various scan rates (20 mV s^{-1}, 40 mV s^{-1}, 60 mV s^{-1}, 80 mV s^{-1}, and 100 mV s^{-1}) in same electrolyte solution on S-2-modified electrode and the result is displayed in Fig. 5. On application of higher scan rates, the electrochemical performance enhances. The cathodic

Table 2 Information from XRD data

Electrocatalysts	Peak position (2θ) (degree)	FWHM (degree)	Planes {hkl}	Crystal size (nm)	Average crystal size (nm)
S-1	38.886	1.2052	{111}	6.492031	5.91
	44.896	1.2402	{200}	6.183396	
	65.106	1.1917	{220}	5.868761	
	78.074	1.2577	{311}	5.124348	
S-2	39.068	0.96824	{111}	9.092895	9.46
	45.198	0.9556	{200}	9.405036	
	65.321	1.0415	{220}	9.463011	
	78.23	1.0787	{311}	9.913898	
S-3	38.667	0.97059	{111}	9.059686	9.57
	44.838	1.0146	{200}	8.8466	
	64.977	1.0108	{220}	9.731739	
	77.908	0.99897	{311}	10.68079	

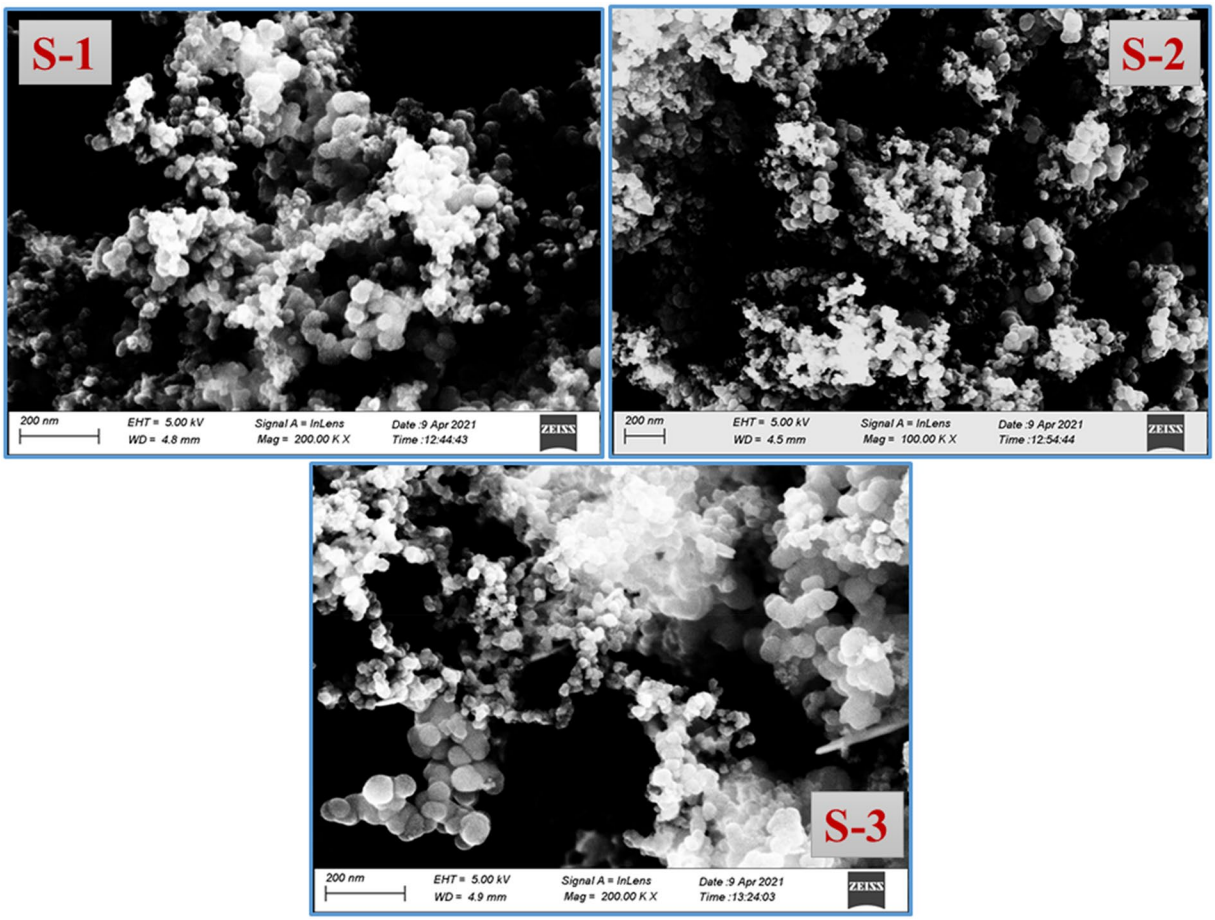

Fig. 2 FESEM image of S-1, S-2, and S-3 electrocatalysts

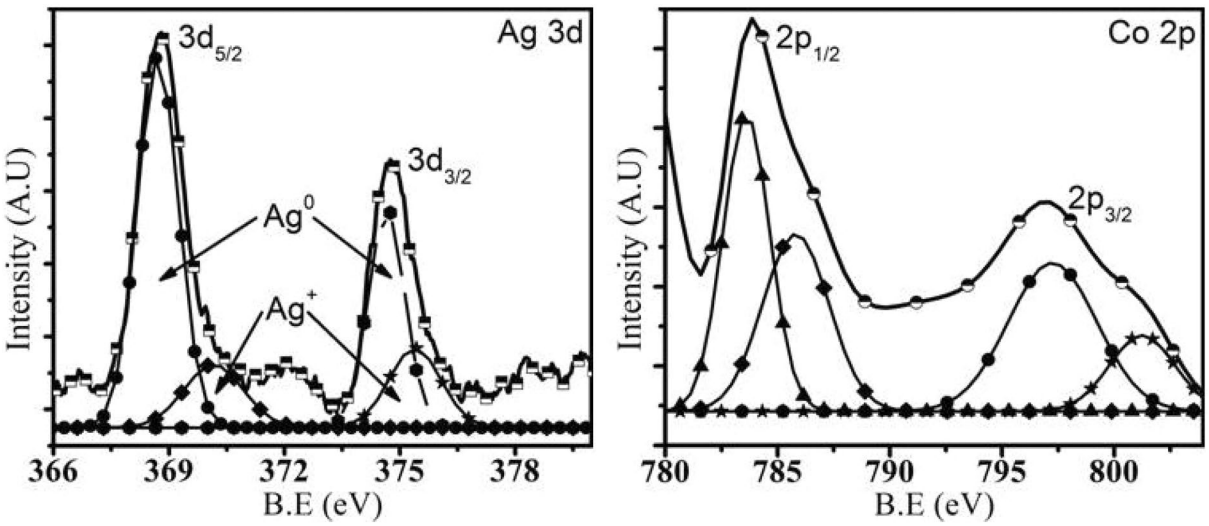

Fig. 3 XPS spectra of Ag 3d and Co 2p region of S-1 electrocatalyst

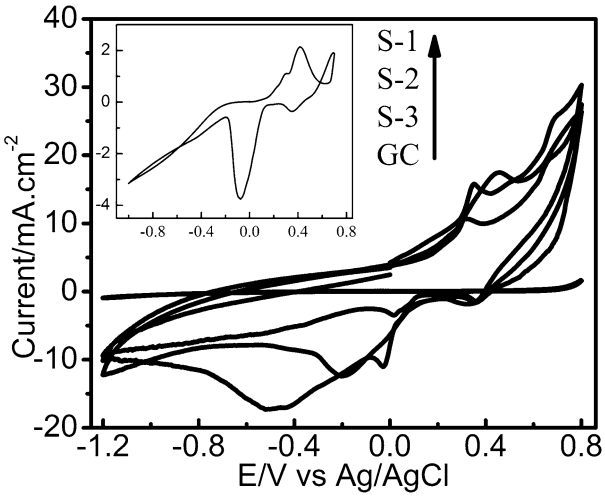

Fig. 4 CV of glassy carbon and all synthesized electrocatalysts in 0.5 M NaOH solution at 100 mV s^{-1} scan rate at 25 °C. Inset shows the CV of Ag/C (20 wt%) at identical conditions

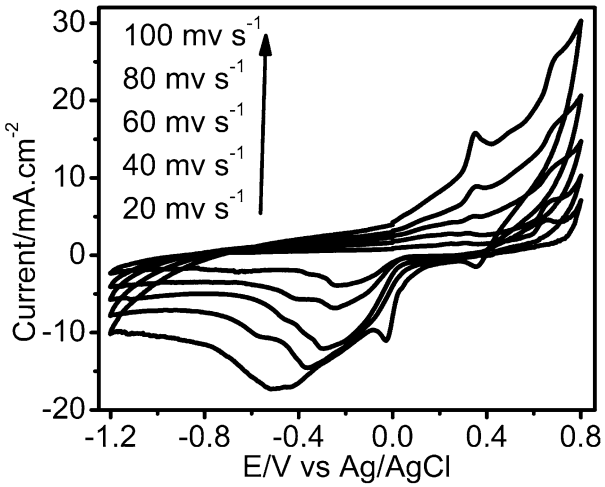

Fig. 5 CV of S-2 electrocatalyst in 0.5 M NaOH solution at different scan rates at 25 °C

and anodic peak potentials move in the further cathodic and anodic directions, respectively, with the increase of scan rates. Both anodic and cathodic peak currents are plotted against the square root of scan rates which is shown in Fig. 6a. Fig. 6b also exhibits the plot of peak potentials versus scan rates. The almost linear relationship in Fig. 6 (a and b both) hints that the oxidation/reduction reaction at Ag–Co/C electrode surface is diffusion-limited process [27].

To study the borohydride oxidation reaction (BOR) kinetics, CV was performed at S-1, S-2, and S-3-modified glassy carbon electrode surfaces in 0.5 M NaOH + 0.01 M $NaBH_4$ at 100 mV s^{-1} scan rate at 25 °C. Figure 7 demonstrates the result of BOR at pure glassy carbon electrode and Ag–Co/C-tailored glassy carbon electrode surfaces. The pure glassy carbon electrode did not exhibit any electrochemical activity toward borohydride oxidation indicating the electrocatalytic inactivity of glassy carbon in alkaline borohydride solution. Generally, BOR at silver-based electrocatalysts is quite complex process which is influenced by the surface oxidation, surface pretreatment, composition of electrolyte ($NaBH_4$ and NaOH concentrations), and particle size [13, 28]. It was noticed that Ag–Co/C electrocatalysts are electrochemically active for borohydride oxidation as confirmed by appearance of extra forward peaks compared to those measured in 0.5 M NaOH solution and by enhanced currents. Current densities evaluated at S-1-decorated glassy carbon electrode were larger than those at other modified electrode surfaces, signifying better electrocatalytic activity in presence of $NaBH_4$. Higher surface-to-volume ratio is a very prominent factor for good electrocatalytic activity. The S-1 electrocatalyst has higher surface-to-volume ratio because of its very smaller size 5.91 nm (surface-to-volume ratio is inversely proportional to size) and presence of higher amount of porous carbon. This is possibly the main cause of its well electrocatalytic performance [29].

The most negative open-circuit potential (OCP) was noticed at S-1-modified electrode surface (around − 0.4 V versus Ag/AgCl), followed by S-2 and S-3 electrocatalyst. It was observed that the value of all OCP was more positive than the value of theoretical equilibrium potential (− 1.24 V vs NHE or approximately − 0.6 V vs Ag/AgCl), mainly due to the presence of mixed potential arising from the hydrolysis of BH_4^- (imparting hydrogen evolution) on Ag surface and following hydrogen oxidation and/or the surface oxide reduction [13]. Forward peaks located at 0.17 V and 0.69 V for S-1 electrocatalyst were corresponded to the electro-oxidation reaction of hydrogen and $NaBH_4$, respectively. The peak at 0.17 V was observed because of the oxidation of H_2 that is generated by the hydrolysis of BH_4 following the reaction (3) [30]:

$$BH_4^- + 4H_2O \rightarrow B(OH)_4^- + 4H_2 \quad (3)$$

Another peak at 0.39 V corresponds to the formation of silver oxide and the peak located at 0.69 V in anodic scan was noticed due to the direct BH_4^- electro-oxidation on S-1 catalyst followed by hydrogen and BO_2 generation [13]. The current density continuously improved with the formation of silver oxide, and the direct electro-oxidation of BH_4^- happened upon Ag_2O multilayer. The mechanism can be expressed by the following equations [31]:

$$2Ag + 2OH^- \rightarrow Ag_2O + H_2O + 2e^- \quad (4)$$

$$Ag_2O + BH_4^- + 6OH^- \rightarrow 2Ag + BO_2^- + 5H_2O + 6e^- \quad (5)$$

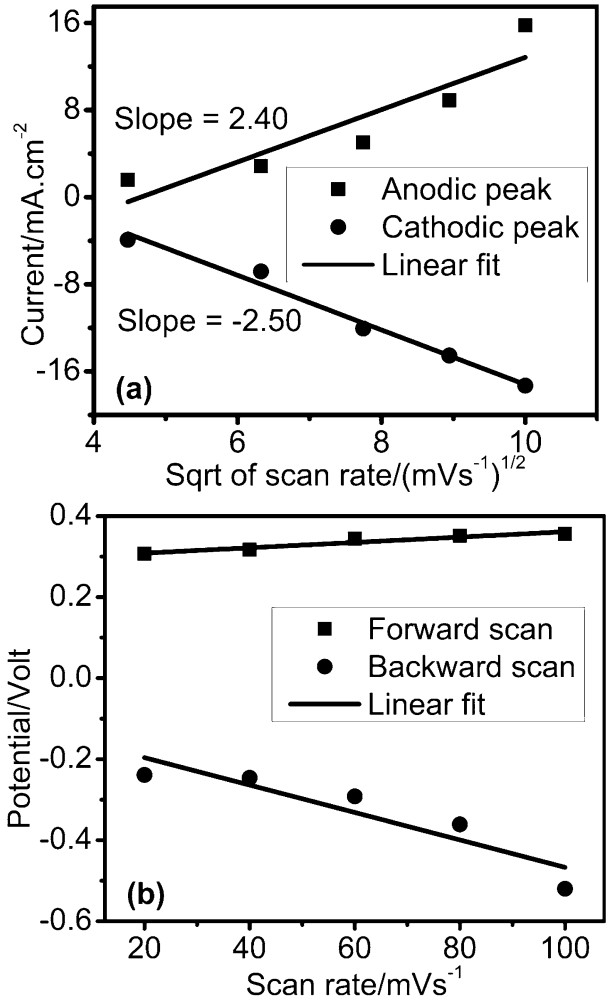

Fig. 6 **a** Plot of square root of scan rates vs current density for S-2 electrocatalyst in 0.5 M NaOH solution at 25 °C. **b** Plot of scan rate vs peak potential for S-2 electrocatalyst in 0.5 M NaOH solution at 25 °C

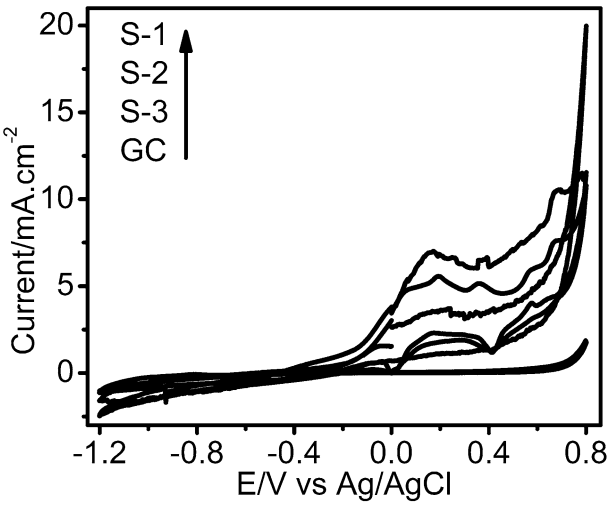

Fig. 7 CV of glassy carbon and all synthesized electrocatalysts in 0.5 M NaOH + 0.01 M $NaBH_4$ solution at 100 mV s^{-1} scan rate at 25 °C

The S-2-modified glassy carbon electrode showed the similar fashion of CV for borohydride oxidation having relatively lower current density than that of S-1 electrocatalyst. In the backward sweep of potential, both S-1 and S-2 catalysts showed two reduction peaks around 0.41 V and − 0.002 V. These peaks were arisen due to the reduction of silver oxides. In case of S-3-tailored electrode, both H_2 and $NaBH_4$ oxidation peaks combined to be a single broad hump and there was no reduction spike in negative potential sweep. The most poor electrocatalytic performance toward BOR was found on S-3-modified electrode. Among the all synthesized catalysts, S-1 showed maximum current density for borohydride oxidation reaction. The peak current densities for BOR on S-1, S-2, and few reported catalysts are listed in Table 3. The S-1 catalyst produces larger current density for borohydride electro-oxidation than $Ni_1@Ag_{1.5}$/C and almost similar current density than $Ni_2@Ag_1$/C reported by the Duan's group [31]. The molar concentration of NaOH and $NaBH_4$ was few times lower in our work than that used by Duan's group [31]. So in terms of current density, our prepared S-1 electrocatalyst is more favorable for borohydride oxidation in alkaline medium.

Investigating the reaction kinetics of electrode and interfacial process in electrochemical system is much useful to realize the reaction procedure properly. EIS is one of the most informative and commanding tool to investigate the charge transfer kinetics in electro-oxidation reaction. Motivating from this we performed EIS measurements between 10^5 and 0.1 Hz for S-1, S-2, and S-3-modified electrodes in 0.5 M NaOH + 0.01 M $NaBH_4$ electrolyte solution at amplitude of 0.01 V. The obtained Nyquist plots from measured EIS data are shown in Fig. 8. The plots showed arc-like nature mainly in high frequency region. The diameter of impedance arc is associated with the faradic charge transfer resistance (R_c) of electrolyte–electrode interface concerned to the electrochemical activity of catalysts [33]. Only a small part of semi-circular arc was shown due to the limitation of the electrochemical analyzer used here. The values of R_c of different catalysts follow the fashion of S-3>S-2>S-1. The S-1-tailored electrode shows the lowest arc diameter. According to the trend, S-1 electrocatalyst has lowest charge transfer resistance which assist to achieve well-organized charge transfer from the electrode surface to electrolyte and thus improves the electrode kinetics [34]. A roughly linear portion in the low frequency region of Nyquist plot was observed for S-1 and S-2 electrocatalyst. The arc-like part in high frequency region and approximately linear part in low frequency region corresponds to the charge transfer-limited process and diffusion-limited process, respectively

Table 3 The peak current densities of BH_4^- on several electrocatalysts

Electrocatalyst	Electrolyte	Current density	References
Ag/C	2 M NaOH + 0.1 M $NaBH_4$	12.1 mA cm^{-2}	[31]
AB_5-type alloy/Si	1 M NaOH + 0.01 M $NaBH_4$	0.4 mA cm^{-2} mg^{-1}	[32]
$Ni_2@Ag_1/C$	2 M NaOH + 0.1 M $NaBH_4$	11.3 mA cm^{-2}	[31]
$Ni_1@Ag_{1.5}/C$	2 M NaOH + 0.1 M $NaBH_4$	8.1 mA cm^{-2}	[31]
S-2	0.5 M NaOH + 0.01 M $NaBH_4$	7.5 mA cm^{-2}	This work
S-1	0.5 M NaOH + 0.01 M $NaBH_4$	10.5 mA cm^{-2}	This work

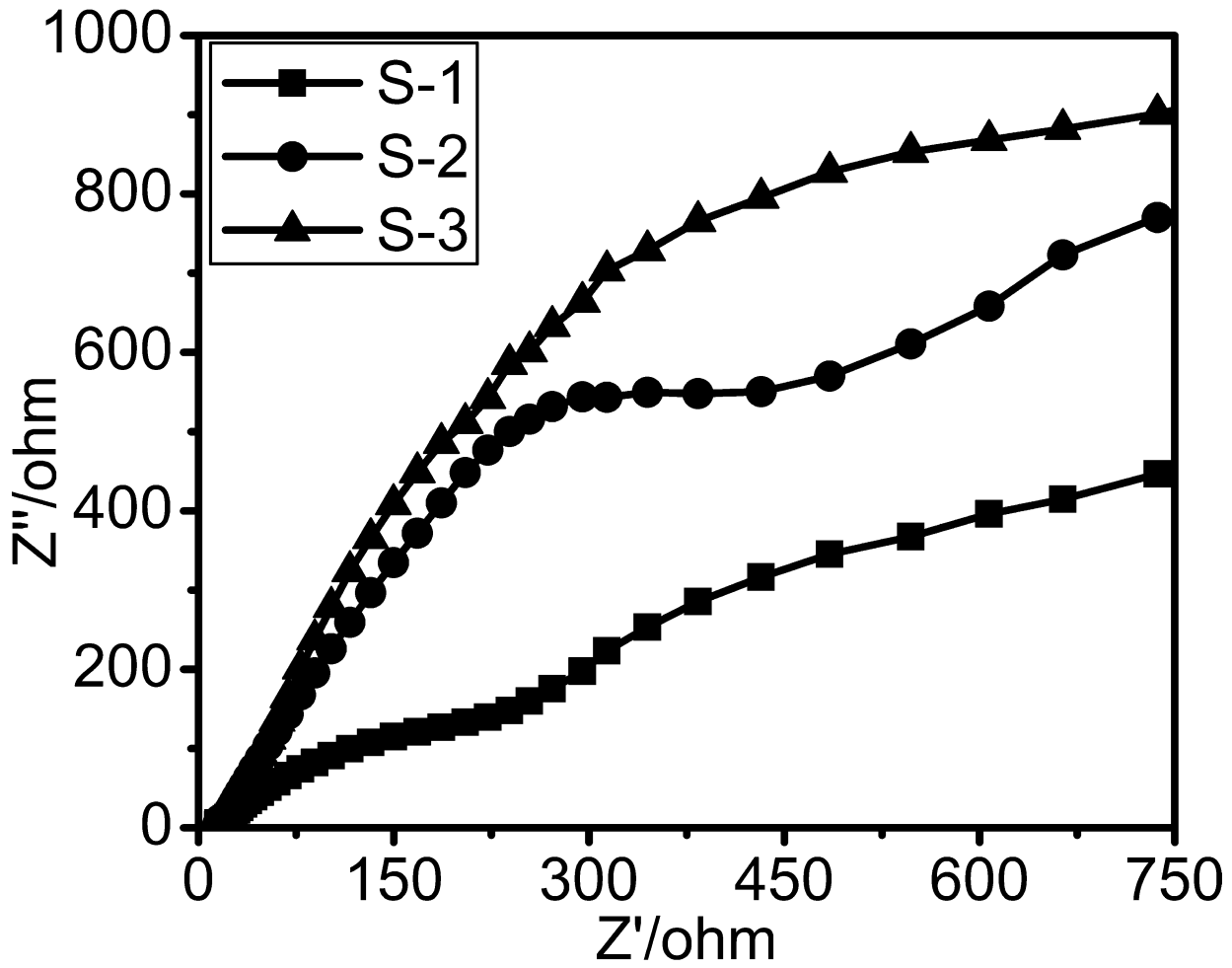

Fig. 8 EIS in 0.5 M NaOH + 0.01 M $NaBH_4$ solution for all electrocatalysts at 25 °C

[35]. These results demonstrate that both electron transfer limiting and diffusion limiting processes exist for the three electrodes.

To harmonize with the CV and EIS study on the electrocatalytic activity and stability test of Ag–Co/C-decorated electrodes in alkaline borohydride solution, CA was explored. Figure 9a represents the CA profile of S-1, S-2, and S-3 catalysts in 0.2 V in 0.5 M NaOH + 0.01 M $NaBH_4$ solution at 25 °C. In the earliest phase of CA profile, a quick current decay was observed due to the absorbance of species on electrode diffusion layers [36, 37]. After that rapid decay, the almost constant current values were noticed indicating the stability of the electrocatalysts [38]. After 650 s, the highest value of current 0.76 mA cm^{-2} was

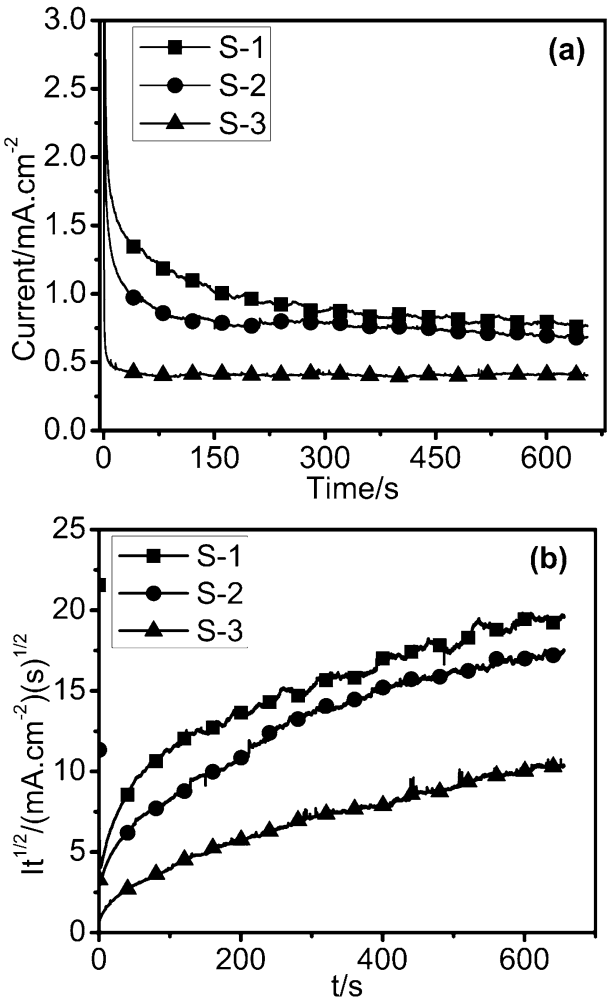

Fig. 9 **a** CA curves of all electrocatalysts in 0.5 M NaOH solution at 0.2 V at 25 °C. **b** Corresponding Cottrell plot ($It^{1/2}$ vs t) of all electrocatalysts

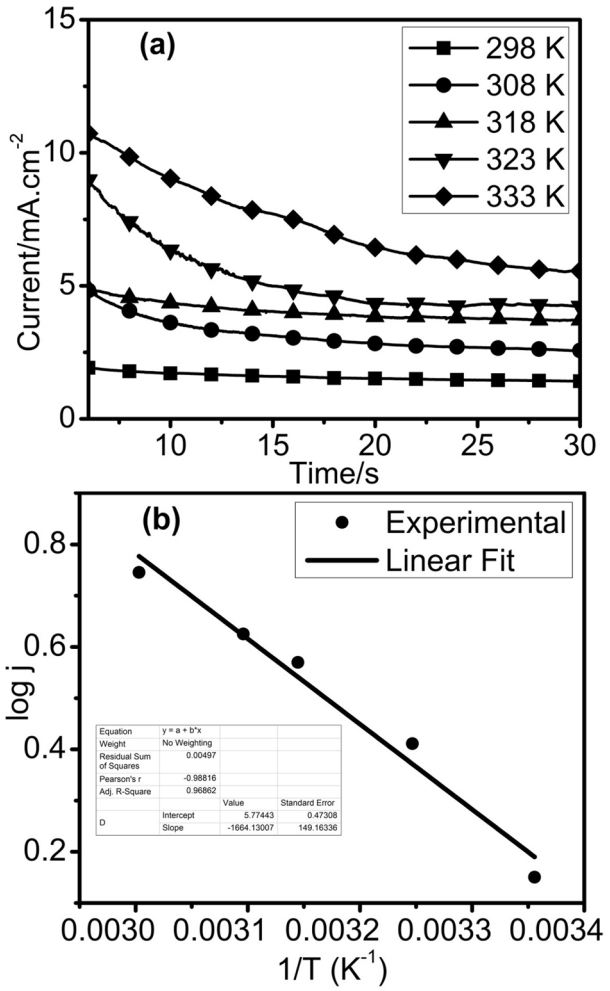

Fig. 10 **a** CA curves of all electrocatalysts in 0.5 M NaOH + 0.01 M $NaBH_4$ solution at 0.2 V at different temperatures. **b** Corresponding plot of log *j* vs 1/*T*

found on S-1 catalyst, trailed by S-2 (0.68 mA cm^{-2}) and S-3 (0.40 mA cm^{-2}), hinting the best electrocatalytic performance of S-1 among the prepared samples in alkaline borohydride fuel cell. Figure 9b demonstrates the Cottrell plot ($It^{1/2}$ versus t) obtained from the CA results. In this figure, the raise of $It^{1/2}$ function is moreover a suggestion that prepared electrode surfaces are not poisoned for the duration of the experiment [39]. Furthermore, the highest $It^{1/2}$ value of S-1 catalyst again hints the most excellent electrocatalytic performance among the synthesized catalysts in alkaline borohydride fuel cell.

The CA was investigated for S-1-modified electrode in 0.2 V in 0.5 M NaOH + 0.01 M $NaBH_4$ solution in 25–60 °C temperature range (Fig. 10a). It is noticed that current density is in increasing fashion with the increase of temperature suggesting that the electrochemical reaction kinetics become quicker at higher temperatures. But the high-temperature CA

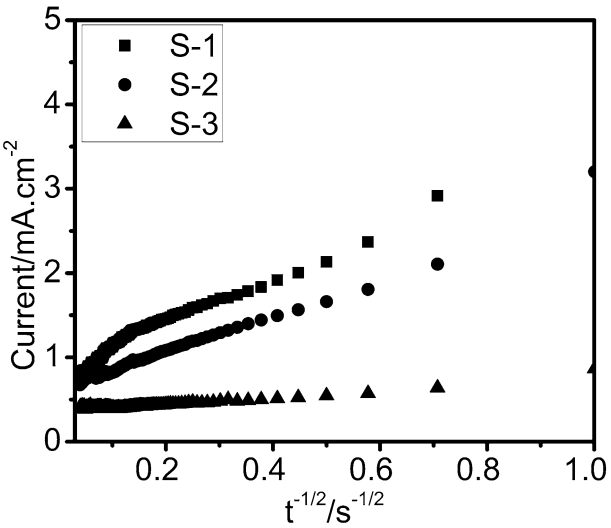

Fig. 11 Plot of current density vs $t^{-1/2}$ from CA data of all electrocatalysts in 0.5 M NaOH + 0.01 M $NaBH_4$ solution

displayed a minor attenuation that may be due to the unrelenting utilization of fuel during the experiment. Again, the $NaBH_4$ hydrolysis rate will be improved and will generate more H_2 gas at the high temperature [40, 41]. The H_2 gas moves away from the electrode surface that can disturb the stability of electrolyte. The apparent activation energy E_{app} of S-1-tailored electrode in 0.5 M NaOH + 0.01 M $NaBH_4$ solution was calculated using Arrhenius equation (Eq. 6):

$$\frac{\partial \log j}{\partial T} = -\frac{E_{app}}{RT^2} \tag{6}$$

where j, T, and R are the current density (mA cm^{-2}), temperature (K), and molar gas constant (8.314 J mol^{-1} K^{-1}), respectively. Figure 10b displays the Arrhenius plot (log j versus 1/T) with a slope value -1664. Using this slope value we obtained the E_{app} of S-1 catalyst in 0.5 M NaOH + 0.01 M $NaBH_4$ solution was 31.86 kJ mol^{-1}. This value is comparable or lower than the values reported on several electrocatalysts, such as Ag/C, $Ni_1@Ag_{1.5}$/C, $Ni_{1.5}@Ag_1$/C, and $Ni_2@Ag_1$/C (42.22, 40.37, 33.83, and 34.75 kJ mol^{-1}) [31].

Number of exchange electrons (n) is an important parameter to study the electrochemical kinetics of catalyst which can be evaluated by analyzing the CA data using Cottrell equation (Eq. 7):

$$j = \frac{nFC\sqrt{D}}{\sqrt{(\pi t)}} \tag{7}$$

where F, C, and D are the Faraday constant (96,485 C mol^{-1}), BH_4^- concentration, and diffusion coefficient, respectively. Wang et al. [42] reported the values of D in different NaOH concentrations at various temperatures considering that D is independent to BH_4^- concentration. The slope values of j versus $t^{-1/2}$ plot (Fig. 11) were found as 4.6, 2.6, and 0.4 for S-1, S-2, and S-3-tailored electrodes in 0.5 M NaOH + 0.01 M $NaBH_4$ solution at 25 °C. Using these slope values and Cottrell equation (Eq. 7), the n values for S-1, S-2, and S-3 catalysts in 0.5 M NaOH + 0.01 M $NaBH_4$ solution at 25 °C were calculated as 1.95, 1.10, and 0.17, respectively. The values of n less than 8 signify the limited anodic oxidation of BH_4^-, with loss of available electrons primarily owing to BH_4^- hydrolysis. Other reported values of n for BOR at $Pt_{0.4}Dy_{0.6}$ and $Pt_{0.5}Dy_{0.5}$-modified electrodes are 2.5 and 2.4, respectively [43].

4 Conclusion

In this work, carbon-supported silver–cobalt (Ag–Co/C) nanoparticles with three different metal-to-carbon ratios were synthesized by reduction method in aqueous solution. The as-prepared electrocatalysts (S-1, S-2, and S-3) exhibited good electrocatalytic performance toward borohydride oxidation in alkaline medium. The S-1 catalysts showed better electrocatalytic performance than S-2 and S-3 as an anode in DBFC in terms of current density, charge transfer resistance, and durability due to its larger surface-to-volume ratio. The effect of temperature on electrocatalytic activity was studied which indicates the enhancement of electro-oxidation dynamics with temperature. The maximum current density at 25 °C temperature and apparent activation energy of S-1-tailored electrode in this study was evaluated as 10.5 mA cm^{-2} and 31.86 kJ mol^{-1}. Thus, the Ag–Co/C nanoparticles with low cost and well performance are supposed to be a hopeful anode electrocatalyst in DBFC.

Acknowledgements The authors would like to acknowledge National Institute of Technology, Durgapur for the financial support through TEQIP program. The authors also want to thank Center of Excellence (COE) for providing characterization facilities.

References

1. Eisa T, Mohamed HO, Choi YJ, Park SG, Ali R, Abdelkareem MA, Oh SE, Chae KJ (2020) Nickel nanorods over nickel foam as standalone anode for direct alkaline methanol and ethanol fuel cell. Int J Hydrogen Energy 45(10):5948–5959
2. Pan Z, Bi Y, An L (2020) A cost-effective and chemically stable electrode binder for alkaline-acid direct ethylene glycol fuel cells. Appl Energy 258:114060
3. Braesch G, Oshchepkov AG, Bonnefont A, Asonkeng F, Maurer T, Maranzana G, Savinova ER, Chatenet M (2020) Nickel 3D structures enhanced by electrodeposition of nickel nanoparticles as high performance anodes for direct borohydride fuel cells. ChemElectroChem 7(7):1789–1799
4. Ma J, Sahai Y, Buchheit RG (2010) Direct borohydride fuel cell using Ni-based composite anodes. J Power Sources 195(15):4709–4713
5. Zhang D, Ye K, Yin J, Cheng K, Cao D, Wang G (2014) Low-cost and binder-free, paper-based cobalt electrode for sodium borohydride electro-oxidation. New J Chem 38(11):5376–5381
6. Evans GE, Kordesch KV (1967) Hydrazine-air fuel cells: hydrazine-air fuel cells emerge from the laboratory. Science 158(3805):1148–1152
7. Zhang Y, Janyasupab M, Liu CW, Li X, Xu J, Liu CC (2012) Three dimensional PtRh alloy porous nanostructures: tuning the atomic composition and controlling the morphology for the application of direct methanol fuel cells. Adv Func Mater 22(17):3570–3575
8. Xu CW, Wang H, Shen PK, Jiang SP (2007) Highly ordered Pd nanowire arrays as effective electrocatalysts for ethanol oxidation in direct alcohol fuel cells. Adv Mater 19(23):4256–4259
9. Han SB, Song YJ, Lee YW, Ko AR, Oh JK, Park KW (2011) High-performance hydrogen fuel cell using nitrate reduction reaction on a non-precious catalyst. Chem Commun 47(12):3496–3498
10. Oliveira RC, Vasić M, Santos DM, Babić B, Hercigonja R, Sequeira CA, Šljukić B (2018) Performance assessment of a direct borohydride-peroxide fuel cell with Pd-impregnated faujasite X zeolite as anode electrocatalyst. Electrochim Acta 269:517–525

11. Liu X, Yi L, Wang X, Su J, Song Y, Liu J (2012) Graphene supported platinum nanoparticles as anode electrocatalyst for direct borohydride fuel cell. Int J Hydrogen Energy 37(23):17984–17991
12. Atwan MH, Macdonald CL, Northwood DO, Gyenge EL (2006) Colloidal Au and Au-alloy catalysts for direct borohydride fuel cells: electrocatalysis and fuel cell performance. J Power Sources 158(1):36–44
13. Stoševski I, Krstić J, Milikić J, Šljukić B, Kačarević-Popović Z, Mentus S, Miljanić Š (2016) Radiolitically synthesized nano Ag/C catalysts for oxygen reduction and borohydride oxidation reactions in alkaline media, for potential applications in fuel cells. Energy 101:79–90
14. Concha BM, Chatenet M (2009) Direct oxidation of sodium borohydride on Pt, Ag and alloyed Pt–Ag electrodes in basic media. Part I: bulk electrodes. Electrochim Acta 54(26):6119–6129
15. Wang GJ, Gao YZ, Wang ZB, Du CY, Wang JJ, Yin GP (2010) Investigation of PtNi/C anode electrocatalysts for direct borohydride fuel cell. J Power Sources 195(1):185–189
16. Feng RX, Dong H, Cao YL, Ai XP, Yang HX (2007) Agni-catalyzed anode for direct borohydride fuel cells. Int J Hydrogen Energy 32(17):4544–4549
17. Šljukić B, Milikić J, Santos DMF, Sequeira CAC (2013) Carbon-supported $Pt_{0.75}M_{0.25}$ (M= Ni or Co) electrocatalysts for borohydride oxidation. Electrochim Acta 107:577–583
18. Demirci UB, Miele P (2014) Reaction mechanisms of the hydrolysis of sodium borohydride: a discussion focusing on cobalt-based catalysts. Comptes Rendus Chimie 17(7–8):707–716
19. Cheng X, Ye K, Zhang D, Cheng K, Li Y, Wang B, Wang G, Cao D (2015) Methanol electrooxidation on flexible multi-walled carbon nanotube-modified sponge-based nickel electrode. J Solid State Electrochem 19(10):3027–3034
20. Hernández-Rodríguez MA, Goya MC, Arévalo MC, Rodríguez JL, Pastor E (2016) Carbon supported Ag and Ag–Co catalysts tolerant to methanol and ethanol for the oxygen reduction reaction in alkaline media. Int J Hydrogen Energy 41(43):19789–19798
21. Chakraborty P, Dey S, Basu S (2021) Structural, electrical and magnetic properties of Eu doped $YCrO_3$ nanoparticles. Phys B Condensed Matter 601:412677
22. Cheng Y, Li W, Fan X, Liu J, Xu W, Yan C (2013) Modified multi-walled carbon nanotube/Ag nanoparticle composite catalyst for the oxygen reduction reaction in alkaline solution. Electrochim Acta 111:635–641
23. Verma A, Gupta RK, Shukla M, Malviya M, Sinha I (2020) Ag–Cu bimetallic nanoparticles as efficient oxygen reduction reaction electrocatalysts in alkaline media. J Nanosci Nanotechnol 20(3):1765–1772
24. Lemke AJ, O'Toole AW, Phillips RS, Eisenbraun ET (2014) The effect of high anionomer loading with silver nanowire catalysts on the oxygen reduction reaction in alkaline environment. J Power Sources 256:319–323
25. He G, Li J, Li W, Li B, Noor N, Xu K, Hu J, Parkin IP (2015) One pot synthesis of nickel foam supported self-assembly of $NiWO_4$ and $CoWO_4$ nanostructures that act as high performance electrochemical capacitor electrodes. J Mater Chem A 3(27):14272–14278
26. Wang Y, Lu X, Liu Y, Deng Y (2013) Silver supported on Co_3O_4 modified carbon as electrocatalyst for oxygen reduction reaction in alkaline media. Electrochem Commun 31:108–111
27. Lin J, He C, Zhao Y, Zhang S (2009) One-step synthesis of silver nanoparticles/carbon nanotubes/chitosan film and its application in glucose biosensor. Sens Actuators B Chem 137(2):768–773
28. Sanli E, Uysal BZ, Aksu ML (2008) The oxidation of $NaBH_4$ on electrochemicaly treated silver electrodes. Int J Hydrogen Energy 33(8):2097–2104
29. Leontyev IN, Chernyshov DY, Guterman VE, Pakhomova EV, Guterman AV (2009) Particle size effect in carbon supported Pt–Co alloy electrocatalysts prepared by the borohydride method: XRD characterization. Appl Catal A 357(1):1–4
30. Ye K, Ma X, Huang X, Zhang D, Cheng K, Wang G, Cao D (2016) The optimal design of Co catalyst morphology on a three-dimensional carbon sponge with low cost, inducing better sodium borohydride electrooxidation activity. RSC Adv 6(47):41608–41617
31. Duan D, Wang Q, Liu H, You X, Liu S, Wang Y (2016) Investigation of carbon-supported Ni@ Ag core-shell nanoparticles as electrocatalyst for electrooxidation of sodium borohydride. J Solid State Electrochem 20(10):2699–2711
32. Wang L, Ma CA, Mao X (2005) $LmNi_{4.78}Mn_{0.22}$ alloy modified with Si used as anodic materials in borohydride fuel cells. J Alloys Compd 397(1–2):313–316
33. Hansu TA, Caglar A, Sahin O, Kivrak H (2020) Hydrolysis and electrooxidation of sodium borohydride on novel CNT supported CoBi fuel cell catalyst. Mater Chem Phys 239:122031
34. Samanta S, Khilari S, Bhunia K, Pradhan D, Satpati B, Srivastava R (2018) Double-metal-ion-exchanged mesoporous zeolite as an efficient electrocatalyst for alkaline water oxidation: synergy between Ni–Cu and their contents in catalytic activity enhancement. J Phys Chem C 122(20):10725–10736
35. Xi P, Cao Y, Yang F, Ma C, Chen F, Yu S, Wang S, Zeng Z, Zhang X (2013) Facile synthesis of Pd-based bimetallic nanocrystals and their application as catalysts for methanol oxidation reaction. Nanoscale 5(13):6124–6130
36. Maya-Cornejo J, Arjona N, Guerra-Balcázar M, Álvarez-Contreras L, Ledesma-García J, Arriaga LG (2014) Synthesis of Pd–Cu bimetallic electrocatalyst for ethylene glycol and glycerol oxidations in alkaline media. Proc Chem 12:19–26
37. Arjona N, Guerra-Balcazar M, Cuevas-Muniz FM, Alvarez-Contreras L, Ledesma-Garcia J, Arriaga LG (2013) Electrochemical synthesis of flower-like Pd nanoparticles with high tolerance toward formic acid electrooxidation. RSC Adv 3(36):15727–15733
38. Safavi A, Kazemi H, Momeni S, Tohidi M, Mehrin PK (2013) Facile electrocatalytic oxidation of ethanol using Ag/Pd nanoalloys modified carbon ionic liquid electrode. Int J Hydrogen Energy 38(8):3380–3386
39. Yi L, Wei W, Zhao C, Yang C, Tian L, Liu J, Wang X (2015) Electrochemical oxidation of sodium borohydride on carbon supported Pt–Zn nanoparticle bimetallic catalyst and its implications to direct borohydride-hydrogen peroxide fuel cell. Electrochim Acta 158:209–218
40. Liu BH, Li ZP (2009) A review: hydrogen generation from borohydride hydrolysis reaction. J Power Sources 187(2):527–534
41. Zhang D, Ye K, Cheng K, Cao D, Yin J, Xu Y, Wang G (2014) High electrocatalytic activity of cobalt–multiwalled carbon nanotubes–cosmetic cotton nanostructures for sodium borohydride electrooxidation. Int J Hydrogen Energy 39(18):9651–9657
42. Wang K, Lu J, Zhuang L (2005) Direct determination of diffusion coefficient for borohydride anions in alkaline solutions using chronoamperometry with spherical Au electrodes. J Electroanal Chem 585(2):191–196
43. Šljukić B, Milikić J, Santos DM, Sequeira CA, Macciò D, Saccone A (2014) Electrocatalytic performance of Pt–Dy alloys for direct borohydride fuel cells. J Power Sources 272:335–343

Authors and Affiliations

Santanu Dey[1] · Subhamay Pramanik[2] · Pradipta Chakraborty[1,3] · Dhiraj Kumar Rana[1] · Soumen Basu[1]

✉ Soumen Basu
soumen.basu@phy.nitdgp.ac.in

[1] Department of Physics, National Institute of Technology, Durgapur, West Bengal 713209, India

[2] Department of Physics, Sidho Kanho Birsha University, Purulia, West Bengal 723104, India

[3] Department of Physics, Bankura Sammilani College, Bankura, West Bengal 722102, India